PNAS RESEARCH ARTICLE | EARTH, ATMOSPHERIC, AND PLANETARY SCIENCES

Tropical cyclones expand faster at warmer relative sea surface temperature

Danyang Wang[a,1,2], Daniel R. Chavas[a,1], and Benjamin A. Schenkel[b,c,d]

Edited by Richard Rotunno, National Center for Atmospheric Research, Boulder, CO; received November 25, 2024; accepted July 21, 2025

Tropical cyclones are expected to intensify more rapidly with warming, but relatively little work has examined whether they could expand more rapidly with warming, too. Recent theory predicts that peak expansion rate should increase with sea surface temperature (SST), and physical arguments suggest this dependence should be specifically on the relative SST, i.e. the SST difference from the tropical mean. We test this hypothesis with historical observational data, in which SST variations are primarily variations in relative SST. Both average and peak expansion rates are found to systematically increase with relative SST globally across the Northern Hemisphere (27.2 and 37.5 km/d/K) and within each individual basin. Results are robust across both reanalysis and Best Track observational datasets. Uniform-SST aquaplanet simulations show a much weaker dependence of maximum expansion rate on absolute SST, suggesting that the dominant dependence is on relative SST. Hence, mean global warming is not expected to strongly change storm size dynamics, but patterns of sea surface warming may play an important role in determining how storm size, and hence coastal risk, may change in the future. This work can also help improve forecasting of the wind field and its hazards and impacts at landfall.

tropical cyclone | hurricane | global warming | size

Significance

Tropical cyclone (TC) size strongly affects its hazards and impacts. This study shows that observed TC size expands substantially faster over relatively warmer water across the major Northern Hemisphere ocean basins. Expansion rates increase much more slowly with global-mean warming as found in simple model simulation experiments. Hence, ocean regions that warm more quickly are more likely to support storms that expand more rapidly, potentially increasing their potential to cause damage and make forecasting the area of their impacts more difficult.

The size of a tropical cyclone (TC) is important for its damage potential (1), particularly in terms of storm surge (2), rainfall (3–5), and tornado occurrence (6). Understanding the evolution of TC outer size, in conjunction with changes in intensity, also helps us understand how the complete wind field evolves (7–10), as well as the storm central pressure (11) that is a strong predictor of impact risk (12). The outer size of the TC is typically observed to expand gradually during the TC life cycle (13). Idealized f-plane simulations show that TC outer size expands to an equilibrium value over an expansion time scale of O(10 d), much longer than typical time scale of O(1 d) for intensification (14–16).

Hurricane intensification rate has been found to increase quickly with warming in both observations (17, 18) and simulations (19–21), qualitatively consistent with the prediction of intensification theory (22–25) as a response to increased potential intensity (22, 26). Could hurricanes also expand more quickly at warmer SST, too? Recently in September 2024, Category 4 hurricane Helene expanded rapidly in outer size, with the diameter of gale-force winds increasing by over 200 km in 24 h while passing over exceptionally warm water in the Gulf of Mexico 3 to 4 K above the tropical mean. This event highlighted the need to better understand how TC expansion rate may change with warming sea surface temperatures. Such a dependence has been suggested in previous studies (3, 27–29) though it has not been formalized in theory nor comprehensively tested observationally.

Recently, a complete theoretical model was developed for the expansion rate of a hurricane (16), and the model predicts that peak expansion rate should increase with warming. The model identifies the latent heat release (equivalent to precipitation) in excess of net radiative cooling to be the driver of TC outer-size expansion. At the same time, a higher free-tropospheric static stability will reduce expansion rate by reducing radial inflow, as required by the maintenance of TC volume-integrated dry entropy (16). The model prediction was found to closely match idealized experiments on the tropical f-plane with uniform SST. They found that TC peak expansion rate of radius of 8 m/s near surface wind increases with SST by ∼4.3 km/d/K (16) with SST increasing from 293 to 307 K in radiative-convective equilibrium (RCE) conditions, corresponding to a global uniform increase of SST. Moreover, on physical grounds, total precipitation rate within the TC is hypothesized to increase much more rapidly at warmer SST relative to the tropical mean (i.e. "relative SST"), governed by weak-temperature-gradient (WTG)

Author affiliations: [a]Department of Earth, Atmospheric, and Planetary Sciences, Purdue University, West Lafayette, IN 47907; [b]Cooperative Institute for Severe and High-Impact Weather Research and Operations, University of Oklahoma, Norman, OK 73072; [c]National Oceanic and Atmospheric Administration, Oceanic and Atmospheric Research National Severe Storms Laboratory, Norman, OK 73072; and [d]School of Meteorology, University of Oklahoma, Norman, OK 73072

Author contributions: D.W. and D.R.C. designed research; D.W. performed research; D.W. and D.R.C. analyzed data; and D.W., D.R.C., and B.A.S. wrote the paper.

The authors declare no competing interest.

This article is a PNAS Direct Submission.

[1]D.W. and D.R.C. contributed equally to this work.

[2]To whom correspondence may be addressed. Email: wang5571@purdue.edu.

This article contains supporting information online at https://www.pnas.org/lookup/suppl/doi:10.1073/pnas.2424385122/-/DCSupplemental.

Published September 15, 2025.

dynamics (30, 31), than at warmer absolute SST. The argument is based on figure 4 of ref. 31, as well as the WTG-based model of ref. 32 for the tropical atmosphere that successfully predicts the rapid increase in precipitation with warming of relative SST that is seen in observations in the tropics (33). Meanwhile, free-tropospheric static stability is hypothesized to be minimally affected by relative SST but to increase with absolute SST following a Clausius–Clapeyron scaling (16). Taken together, the theory of ref. 16 predicts that expansion rate increases much more rapidly with relative SST warming than absolute SST warming (*SI Appendix*, Fig. S1). Past work has indeed shown that both TC precipitation and TC outer size increase systematically with relative SST (3, 4), though there remains large variance in size as well. However, the dependence of expansion rate on SST, whether relative or absolute, has yet to be tested, which is the focus of this work.

We first use historical data over the past 40 y, during which SST variations are principally relative since the tropical mean has changed minimally, to examine the relationship between TC expansion rate and relative SST. We focus our analysis on cases equatorward of 30°N and sufficiently far from land to minimize effects of land or extratropical interaction. We then use TC tracks from a suite of uniform-SST forced aquaplanet simulation data over a range of global SST values from ref. 34 to test absolute SST variations in isolation in order to further distinguish the role of both types of SST variations. TCs in these aquaplanet simulations follow a consistently smooth evolution expanding gradually as they move from low to high latitudes, which is very convenient for our analysis. See *Materials and Methods* for full details.

Recent observational studies (35, 36) introduced the concept of rapid growth of TC outer size based on a 90th-percentile threshold but did not find SST to be an important contributor when comparing composites that did and did not grow rapidly from North Atlantic (NA) and Western North Pacific (WP) basins equatorward of 40°N. Here, we directly analyze both mean and peak expansion rates as a continuous function of relative SST; we focus our analysis equatorward of 30°N to avoid mid-latitude baroclinic interactions; we expand this analysis to span the Eastern North Pacific (EP), WP, and NA; and we test multiple observational datasets for robustness. Finally, for greater physical understanding and interpretation, we further test the validity of the mechanistic steps that link SST variations to changes in expansion rate based on the theory of ref. 16, and we examine the potential role of secondary eyewalls in our findings.

Results

Northern Hemisphere. The dependence of 48-h expansion rate of the radius of 8 m/s near surface wind (dr_8/dt [km/d]; y-axis) on relative SST (rSST) for NA, EP, and WP basins collectively is shown in Fig. 1*A*; see *Materials and Methods* for details on the calculation of each quantity. Results are shown both for all valid 48-h periods (blue) and for storm-maximum expansion rate (red). The 48-h time window is an appropriate time scale for analyzing expansion considering the relatively slow (>1 d) time scale of TC expansion as noted above. Expansion rates are found to increase at a rate of 27.2 km/d/K of rSST warming. Maximum expansion rate is found to increase more rapidly at a rate of 37.5 km/d/K of rSST warming. This effect of rSST on expansion rate in nature is large: For 1 K relative warming, expansion rate increases by 27.2 km/d, which is large in magnitude compared to the median of all expansion rates of 9 km/d. Similarly, for 1 K relative warming, maximum expansion rate increases by 37.5 km/d, which is comparable in magnitude to the median of maximum expansion rates of 56 km/d. Hence, a warmer rSST accelerates the expansion process, particularly at the extremes, and this dependence is of practical importance in operational forecasting.

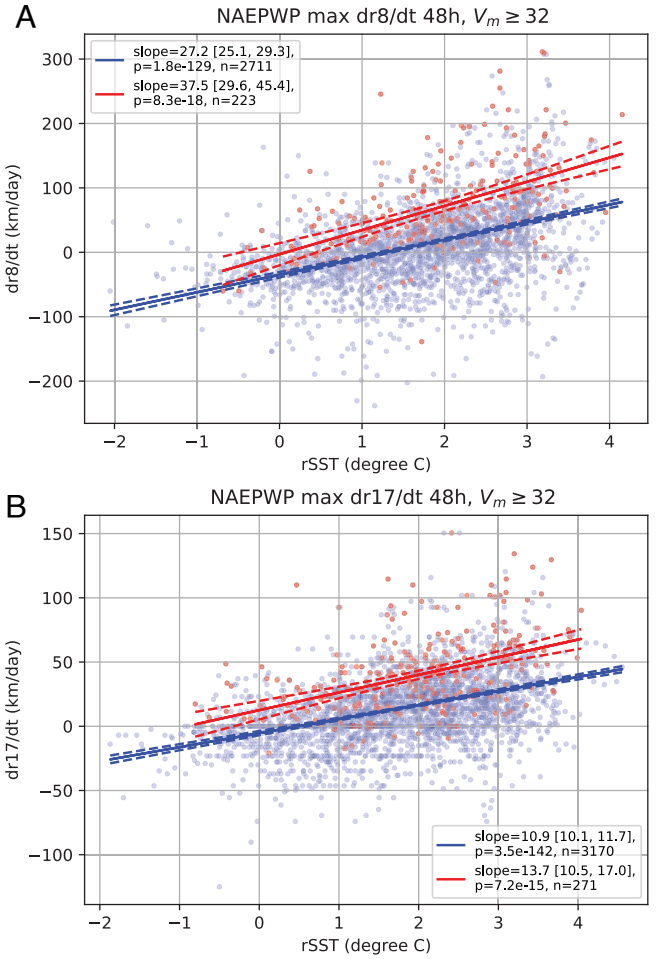

Fig. 1. Tropical cyclones expand faster over water that is warmer relative to the tropical mean. (*A*) 48-h expansion rate of the radius of 8 m/s winds (dr_8/dt [km/d]; y-axis) vs. rSST (x-axis; degrees Celsius) for all Northern Hemisphere (NA, EP, WP) storms, for all valid data (blue) and storm-maximum expansion rate (red). Solid lines are linear regression fits and dashed lines 95% regression confidence band; regression slope, 95% CI, *P*-value (*t* test), and sample size shown in legend. r_8 is estimated from ERA5 reanalysis data. (*B*) Same as (*A*), but for the radius of gale force winds (r_{17}) from Best Track data.

This qualitative result is confirmed using Best Track r_{17} (radius of 17.5 m/s or 34 kt near surface wind) as well (Fig. 1*B*). Expansion rates are found to increase at a rate of 10.9 km/d/K of rSST warming. Maximum expansion rate is found to increase more rapidly at a rate of 13.7 km/d/K of rSST warming. This effect is again large: For 1 K relative warming, expansion rate increases by 10.9 km/d, which is comparable in magnitude to the median of all expansion rates of 12 km/d. Similarly, for 1 K relative warming, maximum expansion rate increases by 13.7 km/d, comparable in magnitude to the median of maximum expansion rates of 35 km/d. Results are qualitatively similar when using a 24-h time window for expansion (*SI Appendix*, Figs. S2 and S3). Note that the rate of change per rSST (for all 48-h expansion periods) is smaller than the median value for r_{17} but is larger than median value for r_8. The larger dependence of expansion rate on rSST for r_8 than r_{17} could be partly contributed

by the more sensitive response of precipitation from r_{17} to r_8 (outer rainband) than the response within r_{17} (*SI Appendix*, Fig. S4); this is consistent with previous studies suggesting that outer spiral rainbands are important for TC outer-size expansion (14, 15, 37–39).

Individual Basins and Subbasins. We next examine whether the rSST dependence of expansion rate found above collectively for the Northern Hemisphere is also found within the individual basins. The analysis in Fig. 1 is repeated for individual basins in Fig. 2. For the North Atlantic ("NA"), we further examine the open ocean portion of the North Atlantic ("NA-OO") east of the Caribbean and the Gulf of Mexico subbasin ("NA-GoM") given their geographic separation by land (Caribbean, Cuba, and Florida) and the practical interest in the Gulf of Mexico as a region where nearly every hurricane will make landfall and impact society.

The results for r_8 are shown in Fig. 2 *A*–*C* and for r_{17} in Fig. 2 *D*–*G*. In the North Atlantic, for r_8 only NA-OO is included as r_8 is too large within the relatively small Gulf of Mexico subbasin to yield any valid cases that meet our quality control criteria away from land (*Materials and Methods*). However, because r_{17} is roughly half the magnitude of r_8, it is small enough to yield a sufficiently large sample size for statistical analysis when using a 24-h period. The tracks of TCs in each subbasin corresponding to r_8 expansion in Fig. 2 *A*–*C* are shown in *SI Appendix*, Fig. S5.

Across basins and subbasins, the outcomes are generally very similar to the aggregated results in Fig. 1*A*. For r_8, expansion rates (blue dots and lines) are found to increase at a rate of 25.8 km/d/K, 24.9 km/d/K, and 34.4 km/d/K of rSST warming in NA-OO, EP, WP, respectively. Maximum expansion rate (red dots and lines) is found to increase at a rate of 21.1 km/d/K, 30.8 km/d/K, and 28.1 km/d/K of rSST warming in NA-OO, EP, and WP, respectively. The effect is substantial: For 1 K relative warming, expansion rate increases by 25.8 km/d, 24.9 km/d, and 34.4 km/d, in NA-OO, EP, and WP, respectively, which is large in magnitude compared to the median of all expansion rates of 19 km/d, −4 km/d, and 17 km/d, in these subbasins, respectively. Similarly, for 1 K relative warming, maximum expansion rate increases by 21.1 km/d, 30.8 km/d, and 28.1 km/d, in NA-OO, EP, and WP, respectively, which is comparable in magnitude to the median of maximum expansion rates of 54 km/d, 32 km/d, and 95 km/d, in these subbasins, respectively. Note that in the EP basin storms typically have the smallest expansion rates, consistent with this basin having the smallest TCs (4) and also the smallest relative SSTs in Fig 2*B*. The same analysis as Fig. 2 *A*–*C* but for a 24-h time window is shown in *SI Appendix*, Fig. S6. Results are qualitatively similar except that the increase of maximum expansion rate with rSST in WP is no longer statistically significant. This appears to be consistent with our consideration that the expansion process is typically a slower process with a time scale of several days and so a 24-h time window for a single period in the storm lifecycle may be more sensitive to shorter-term changes in outer-size due to other environmental factors.

For r_{17} (Fig. 2 *D*–*G*; TC tracks shown in *SI Appendix*, Fig. S7), results are qualitatively similar to r_8 (Fig. 2 *A*–*C*). The lone minor exception is that the storm-maximum expansion rate in the NA-OO increases systematically with rSST but the dependence is not statistically significant (Fig. 2*D*); further discussion is provided in the *Discussion* below. Otherwise, expansion rates (blue dots and lines) are found to increase at a rate of 6.1 km/d/K, 20.5 km/d/K, 10.9 km/d/K, and 12.5 km/d/K of rSST warming in NA-OO, NA-GoM, EP, and WP, respectively. Maximum expansion rate (red dots and lines) is found to increase at a rate of 21.1 km/d/K, 9.9 km/d/K, and 16.5 km/d/K of rSST warming in NA-GoM, EP, and WP respectively. As with prior results, this effect is again large: For 1 K relative warming, expansion rate increases by 6.1 km/d, 20.5 km/d, 10.9 km/d, and 12.5 km/d, in NA-OO, NA-GoM, EP, and WP, respectively, which is comparable in magnitude to the median of all expansion rates of 23 km/d, 23 km/d, 1 km/d, and 16 km/d, in these subbasins, respectively. Similarly, for 1 K relative warming, maximum expansion rate increases by 21.1 km/d, 9.9 km/d, and 16.5 km/d, in NA-GoM, EP, and WP, respectively, which is comparable in magnitude to the median of maximum expansion rates of 32 km/d, 23 km/d, and 52 km/d, in these subbasins, respectively. The signal is slightly weaker in NA-OO but still imposes a significant effect on expansion rate, particularly for >1 K variations in rSST as is common in this subbasin (Fig. 2*D*). The same analysis as Fig. 2 *D*, *F*, and *G* but for 24-h time window is shown in *SI Appendix*, Fig. S8. Results are qualitatively similar except that expansion rate for r_{17} in NA-OO increases with rSST a bit more slowly at 3.6 km/d/K, though remains statistically significant.

The intrabasin findings are overall consistent with the interbasin analysis (Fig. 1), as the mean expansion rate dependence on rSST in each basin is generally comparable across basins and with the full dataset. The storm-maximum expansion rate dependence in each basin is generally smaller than that found when considering all basins together (Fig. 1). This outcome is not surprising given that for storm-maximum expansion, the intrabasin rSST variation (SD 0.69, 0.87, 0.84 K in Fig. 2 *A*–*C*, respectively) is smaller than for all basins combined (SD 0.99 K in Fig. 1*A*). As a result, the rSST dependence may be better estimated by combining all the basins together to span a wider range of rSST.

Dependence on Absolute SST: Uniform-SST Aquaplanet Simulations. To confirm the importance of relative SST against absolute SST, we now test the dependence of expansion rate on absolute SST in a preexisting suite of uniform-SST aquaplanet simulations with a globally uniform SST over a range of SST values from 295 K to 305 K (*Materials and Methods*). In these simple idealized simulations, whose design removes significant large-scale environmental variability (e.g. jet stream), most TCs follow a very simple lifecycle, forming at low latitudes and gradually expanding towards its equilibrium outer size as they move uniformly poleward and westward with time (*SI Appendix*, Fig. S9). The aquaplanet simulations are capable of producing intense TCs, with a distribution of lifetime maximum intensity for the 300 to 301 K simulations (i.e. representative present-day SSTs) similar to that found in observations (*SI Appendix*, Fig. S10). As with the observational datasets, we analyze both expansion rate in general and storm-maximum expansion rate.

Fig. 3*A* shows how maximum 48-h expansion rate of r_8 varies with SST across aquaplanet simulations (one value per storm within each simulation). Maximum expansion rate systematically increases with SST at a relatively slow rate of 2.9 km/d/K. This value is comparable to the 4.3 km/d/K dependence found in idealized f-plane (equivalent to ∼20°N) single-TC simulations with idealized radiation and substantially better resolved TC inner core in ref. 16. Median values of maximum expansion rate (blue lines in Fig. 3*A*) systematically increase with SST consistent with the regression results, except at very warm SSTs where sample sizes are smaller while variance across storms is large. Sample size generally decreases with SST from about 250 at

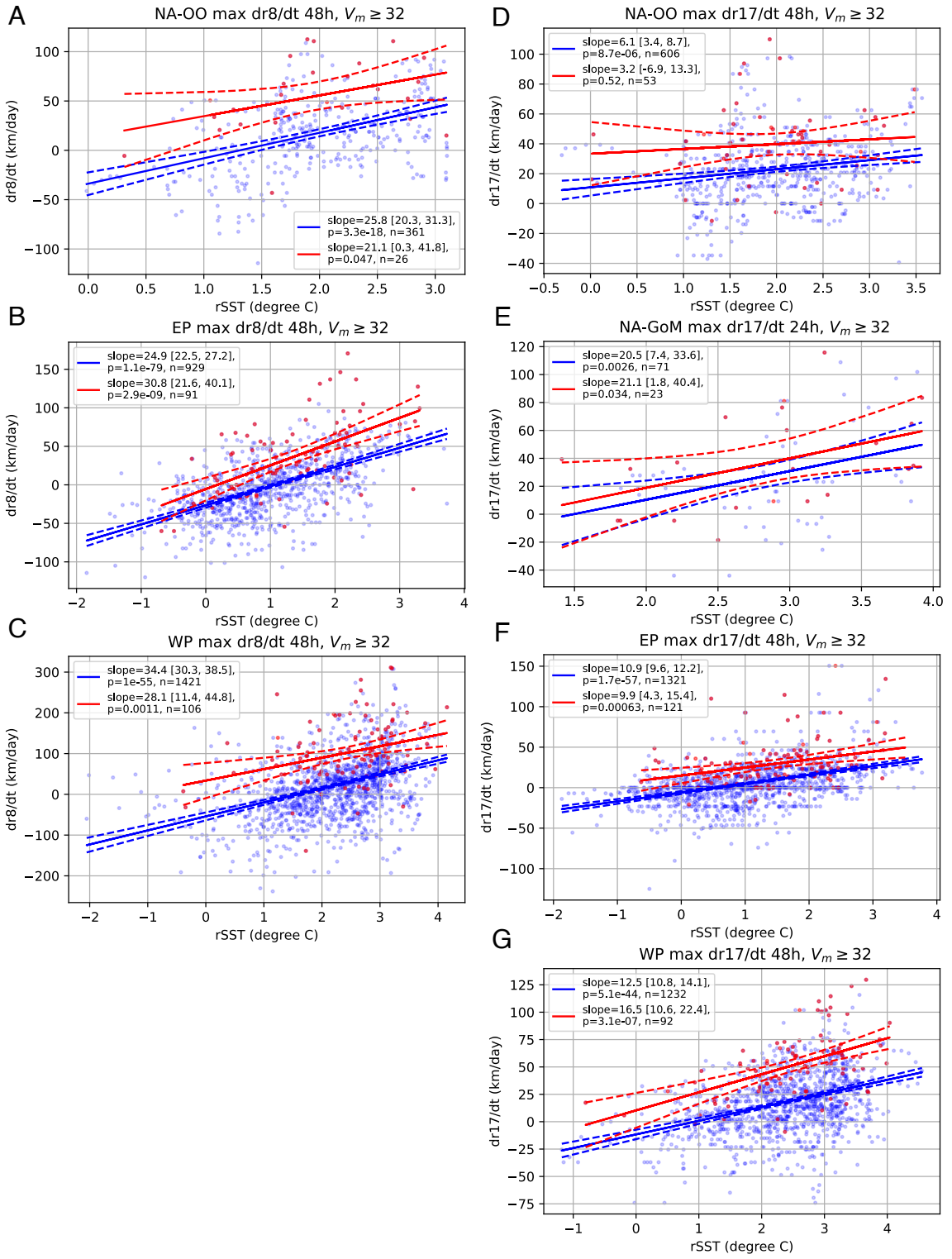

Fig. 2. The dependence holds up within individual basins as well. (*A*–*C*) Same as Fig. 1*A*, but for subbasins: (*A*) NA-OO, (*B*) EP, (*C*) WP. (*D*–*G*) same as Fig. 1*B*, but for subbasins: (*D*) NA-OO, (*E*) NA-GoM (in 24-h time window), (*F*) EP, (*G*) WP.

SST = 295 K to about 35 at SST = 305 K (*SI Appendix*, Fig. S11); tracks shown in *SI Appendix*, Fig. S9 for visualization. Expansion rates in all valid 48 h periods (not only when peak expansion rate occurs) also systematically increase with SST, consistent Fig. 3*A*, but at an even slower rate of 1.8 km/d/K (*SI Appendix*, Fig. S12).

Given that the TC lifecycle is quite simple and smoothly varying in the aquaplanet simulations, we also visualize the dependence of expansion rate on SST via the composite mean evolution of r_8 relative to r_8 = 600 km within each simulation, as shown in Fig. 3*B*. The composite time-series is shown for all times with sample size of at least 10 storms (*SI Appendix*, Fig. S13). The 600 km reference value for radius is chosen simply because it is close to the median value associated with the time of maximum expansion rate (Fig. 3*A*) across SSTs (*SI Appendix*, Fig. S14),

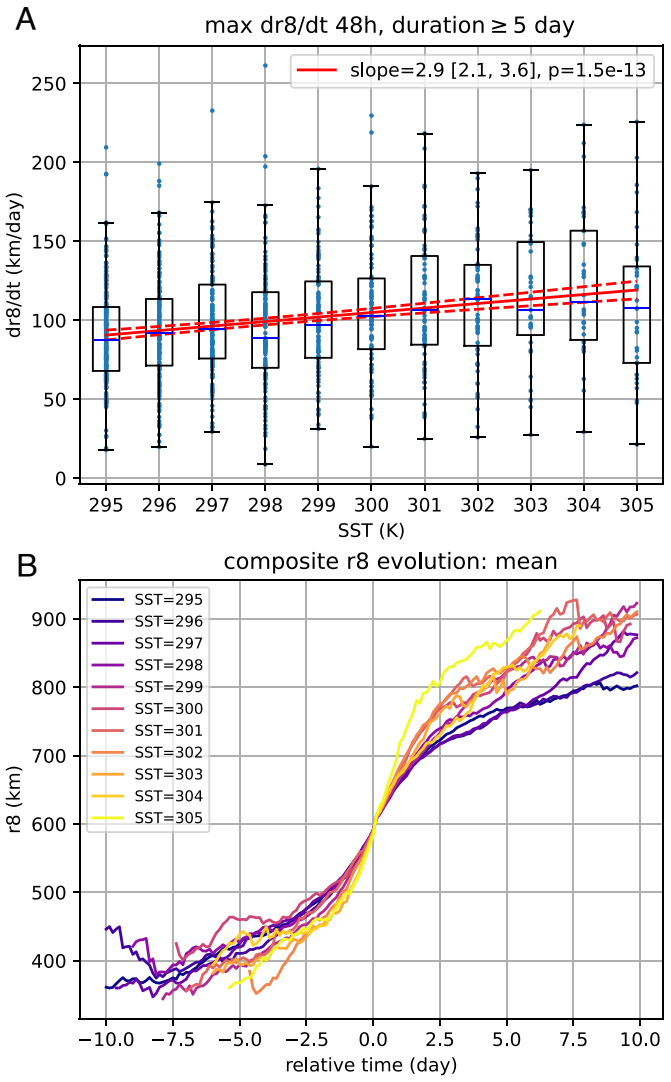

Fig. 3. Expansion rate increases much more slowly with mean warming. Results obtained from the aquaplanet dataset in ref. 34. (*A*) Scatter plot of maximum dr_8/dt (km/d) in the 48-h time window at different SSTs (K). Overlaid is the corresponding box plot showing median, interquartile range (IQR), with whiskers based on 1.5 times the IQR. The red solid line is the linear regression fitting. The slope of the linear regression is shown in legend text with its 95% CIs shown in square brackets; the *P*-value of the slope in the significance test (*t* test) is also shown in legend text (marked by "p"). Red dashed lines show 95% CIs of the mean response of the maximum dr_8/dt (km/d) in the 48-h time window to SST. (*B*) The composite mean evolution of r_8 (km) as a function of time (day) relative to the time of the last r_8 record before r_8 exceeds 600 km for the first time in each TC at a given SST (K; see legend).

indicating that storms expand fastest at an intermediate size as it expands towards its equilibrium size. The composite TC systematically expands more rapidly at warmer SST, increasing from approximately 55 km/d at 295 to 297 K to approximately 80 km/d at 303 to 305 K (*SI Appendix*, Fig. S15).

Hence, the dependence of peak expansion rate on absolute SST found here is much weaker than the dependence on rSST found in historical observations. This outcome supports our primary hypothesis: TCs gradually expand faster with global-mean warming, but expansion rates increase much more rapidly with relative warming.

Testing Hypothesized Mechanism for Contrast in Expansion Rate. To provide greater physical insight into our results above, we test the physical linkages underlying the hypothesis described in Introduction for why expansion rate increases much more rapidly with rSST than absolute SST. There are two core linkages based on the theory (16) for r_8 expansion: 1) precipitation should increase much more rapidly at warmer rSST than absolute SST, following from WTG theory and consistent with the observed distribution tropical precipitation (31–33); 2) enhanced precipitation drives enhanced radial inflow needed to import angular momentum and hence to expand the TC. We utilize the Multi-Source Weighted-Ensemble Precipitation (MSWEP) precipitation dataset (40) (*Materials and Methods*), following ref. 41, combined with ERA5 reanalysis data (42) for low-level (850 hPa, results similar for 925 hPa) radial wind. The test is performed for r_8 for a direct comparison with ref. 16.

First, the theory (16) formally identifies the quantity P_t/r_t, where r_t is the radius of near surface wind speed v_t (not too large, verified at 8 m/s) and P_t is the area integrated precipitation rate (mass per unit time) within r_t, as the driving factor for TC expansion via its direct relationship to low-level radial inflow at r_t (equation 10 of ref. 16). Hence, P_t/r_t should increase more rapidly with relative SST than absolute SST, the latter dependence following Clausius–Clapeyron (C–C) scaling (figure 9c of ref. 16).

SI Appendix, Fig. S16 *A* and *B* shows that a 1 K increase of rSST accounts for a ∼20% increase of P_8/r_8 relative to median P_8/r_8. Results are very similar for the 24 h period and for all expansion periods (*SI Appendix*, Fig. S16). On the other hand, P_8/r_8 was found to increase much slower with absolute SST, approximately following C–C scaling of 6%/K (figure 9c of ref. 16, figure 8d of ref. 34). Direct calculations using the aquaplanet precipitation data (34) gives similar results (∼7%/K; see *SI Appendix*, Fig. S17). These results support the hypothesis for the differing dependence of precipitation on relative vs. absolute SST.

Second, *SI Appendix*, Fig. S16 *C–F* shows the strong link between P_8/r_8 and azimuthal-mean radial inflow at r_8 at 850 hPa as well as between radial inflow and expansion rate in observations, thereby verifying that the expansion mechanism of ref. 16 is consistent with our principal conclusion found above. The required data are not available to test this in the aquaplanet simulations, but the outcome is expected to be the same given its uniform-SST setup directly analogous to the limited-area simulations of ref. 16. These results support the hypothesis for how enhanced precipitation drives expansion mechanistically via enhanced radial inflow.

An additional mechanism in the theory that differentiates variations in relative vs. absolute SST is through bulk free tropospheric static stability, Δs_d, defined as the dry-entropy difference between upper and lower troposphere. The theory (16) indicates that a higher Δs_d will reduce expansion rate by reducing inflow velocity (equation 10 and simulations of ref. 16). The quantity Δs_d should not change with rSST following the WTG theory (30–32) whereas it increases with absolute SST following C–C scaling (figure D3c of ref. 16, and ref. 43). This effect suppresses the increase in expansion rate due to the increase in precipitation at warmer absolute SST. This outcome is verified in *SI Appendix*, Fig. S18, which shows that the dependence of Δs_d (obtained from ERA5 data) on rSST is roughly an order of magnitude smaller than C–C scaling, supporting the proposed mechanism. Such an increase in static stability with warming has been shown in very similar simulations (44).

Role of Secondary Eyewall (SE) Formation and Eyewall Replacement Cycle (ERC). We provide further insights into the expansion process by examining the extent to which SE formation, which

is a precursor to ERCs, contributes to the rSST dependence of expansion rate in historical data (r_{17}), as previous studies have shown that SE and ERC are associated with expansion of outer size (14, 45–48). To do so, we use a public dataset of SE formation from ref. 49, which provides a climatology of 72 TCs that include labels for the time instants with an SE present (*Materials and Methods*), and then infer the importance of ERC as SE formation is a necessary precursor for an ERC.

From among the 72 TCs in the dataset, there are 34 TCs in total available for 48-h expansion analysis for r_{17} after our quality control (36 TCs available for 24-h expansion analysis), with 7 TCs in NA-OO, 10 in EP and 17 in WP. *SI Appendix*, Figs. S19 and S20 indicate that the 34 TCs reach relatively high lifetime maximum intensities (mostly Category 3+) and have a probability of SE occurrence consistent with climatology (45, 50), which indicates that the dataset can be used to estimate the climatological role of SE occurrence in the expansion process.

We repeat the analysis of Fig. 1b using this dataset of TCs from ref. 49, shown in *SI Appendix*, Fig. S21. The dependence of dr_{17}/dt on rSST with all periods removed that contain at least one SE occurrence is similar to the result for the full dataset (for both maximum and all expansion rates). Indeed, SE occurrence is simply relatively infrequent: The number of periods with an SE is much smaller than without (for all expansion periods as well as for peak). The proportion of 24-h periods that include an SE during the TC lifecycle with intensity greater than 32 m/s and equatorward of 30°N is 76/613 $\approx$ 12% (*SI Appendix*, Fig. S21 *d* vs. *b*). For ERCs, which have a typical timescale of 36 h (46), the fraction of TC lifetime influenced by ERC events would then be <18%, though likely significantly less given that SE frequently occurs without inducing a subsequent ERC. This outcome indicates that our results are not strongly driven specifically by SE. Notably, though, we do find that SE substantially accelerates expansion during the brief periods when they occur, with the median of peak 48-h expansion rates increased from 38 km/d to 47 km/d; these events tend to occur at warmer rSST (*SI Appendix*, Fig. S21).

The same analysis cannot be repeated for r_8 in reanalysis data, as there are only 3 TCs in NA-OO, 5 TCs in WP, and 9 TCs in EP available from the ref. 49 dataset that meet our quality control criteria, which is too small to produce meaningful results and is also not representative of individual basins. Such an analysis could be tackled in future work as the SE database grows with time.

Overall, we find that SE, which is a necessary precursor for ERC, can drive especially fast expansion for brief periods during the TC lifecycle. They are relatively infrequent, though, and so are not a primary driver of our results presented here. This outcome also lends greater support for our analysis of aquaplanet simulations whose coarser resolution may not adequately resolve ERC, which is a limitation but is not expected to alter our qualitative findings.

Summary and Discussion

Overall, observational results across NA, EP, WP combined, and within each individual basin confirm that TCs expand substantially faster when over relatively warmer water. This effect is significant on a timescale of 1 to 2 d and hence is important for the real-world forecasting of tropical cyclone size. Maximum expansion rate increases with rSST by about 10 to 20 and 20 to 30 km/d/K in terms of r_{17} (NA-GoM, EP, WP) and r_8 (NA-OO, EP, WP), respectively. This increase in expansion rate for 1 K increase of rSST is significant compared to the typical median value of all storms in each basin or collectively in the Northern Hemisphere. In contrast, maximum expansion rate increases with absolute SST by only about 3 km/d/K for r_8 in uniform-SST aquaplanet simulations, consistent with the theory and limited-area modeling results of ref. 16. This dependence is roughly an order of magnitude smaller than the dependence on rSST, indicating that relative SST is a substantially more important factor for accelerating TC expansion than is absolute SST. Hence, global-mean warming is not expected to cause substantial changes in storm outer-size dynamics, consistent with recent work finding that average storm outer-size itself is not expected to change with mean warming (51, 52). Instead, it is the pattern of warming that likely determines how storm outer-size may change regionally, including near coastlines where changes in storm outer size prior to landfall could translate to changes in societal risk. Given that larger storms tend to cause greater hazards all else equal, this outcome may have important potential implications for changes in coastal risk that are not accounted for in existing risk models and should be studied in future work. Predicting how regional SST patterns will change in the future, including under long-term warming, remains especially challenging though (53). On operational timescales, a more rapid expansion of the storm wind field prior to landfall makes hazard forecasting and evacuation planning more difficult, such as in the recent case of Hurricane Helene (2024) in the Gulf of Mexico that expanded very rapidly two days prior to landfall.

As noted in the Introduction, variation in relative SST is commonly associated with WTG dynamics (30, 31), rather than RCE, which corresponds to a global-mean warming of absolute SST. The faster increase of expansion rate with relative SST compared to absolute SST is consistent with the data-supported hypothesis of different responses of total precipitation rate and radial inflow within the TC and free-tropospheric static stability to relative SST and absolute SST. It follows, by TC outer-size expansion theory in ref. 16 and by *SI Appendix*, Fig. S1, that peak expansion rate should depend more strongly on SST in WTG dynamics than RCE as found here. Tests with a model that is explicitly forced to be in WTG could provide further robustness for our findings.

Both the uniform-SST aquaplanet simulations of ref. 34 and the single TC experiments of ref. 16 are designed not to include any mid-latitude baroclinicity and monsoons so as to isolate the effect of absolute SST. Including these synoptic flows in future studies could help clarify how interactions between the TC and upper-tropospheric troughs/monsoonal flows, that may influence TC size dynamics as well (54–57), could also change with absolute warming.

The lack of a strong dependence of expansion rate of r_{17} on relative SST in the NA-OO is unclear but an important avenue for future work. Indeed, the real world is complicated, so other mechanisms independent of rSST that are known to drive rapid expansion may also be at play (58). This may include extratropical interaction (56, 57), land interaction, or TC internal structural variability such as eyewall replacement cycles (45, 46), all of which are known to occur frequently in the Western Atlantic.

Materials and Methods

Observational SST. Observational SSTs are taken from the Optimum Interpolation SST (OISST) dataset (59), which is based on both in situ and satellite observations and has a daily temporal resolution starting from September 1981 to present with a relatively high spatial resolution of 0.25°.

Definition of Basins. For observational data (best-track and reanalysis), we focus on three major basins in the northern hemisphere: North Atlantic (NA), Eastern North Pacific (EP), and Western North Pacific (WP). The definitions of basins are simplified from those in International Best Track Archive for Climate Stewardship (IBTrACS) (60) data. Specifically, NA has an eastern boundary at 30°W and a western boundary being the blue line in *SI Appendix*, Fig. S22 (this western boundary only applies to ref. 61 reanalysis data); EP is defined west of the blue line in *SI Appendix*, Fig. S22 (this eastern boundary only applies to ref. 61 reanalysis data) and east of 180°E; WP has eastern and western boundaries of 100°E and 180°E. The NA and EP definition only applies as a further constraint for "Extended Best Track" (EBT) dataset, based on the original separation of basins in EBT dataset. The EBT dataset for central pacific is also included for EP analysis in the present study. We further define two subbasins in NA, the Gulf of Mexico (NA-GoM) and open ocean (NA-OO). NA-GoM is defined to be 100°W to 80°W in longitude and 18°N to 30°N in latitude. NA-OO is all the other area of NA basin. The basin to which a TC belongs is assigned by the first record of latitude and longitude of the TC. Occasionally a TC that originally formed in EP can travel into WP, so for simplicity we discard TCs that form in EP but enter WP while still equatorward of 30°N.

Best-Track Data and Processing. Track, intensity, and size data are obtained from the 6-hourly "Extended Best Track" data (62) for the North Atlantic (NA) basin for 1988–2021 and the Eastern North Pacific (EP) basin for 1990–2021. TC outer size is defined as the radius of 34 kt (17.5 m/s; r_{17}) near surface winds, which is the outermost wind radius that is routinely estimated operationally. r_{17} is an excellent representative measure of overall storm size and can be readily estimated via remote sensing instruments (8, 9, 11). Extended Best Track is identical to the National Hurricane Center Best Track database but includes r_{17} data prior to 2004. For the Western North Pacific, data are obtained from the Joint Typhoon Warning Center data in IBTrACS (60) for the period 2001–2022 (3 hourly). Data from the Western North Pacific basin are likely a bit less robust due to the absence of aircraft reconnaissance as is routinely performed in the western North Atlantic and Eastern Pacific basins; however, r_{17} can still be estimated operationally from most satellite remote sensing platforms that have been active over the past three decades (63). The chosen periods extend back to the first year with size data available in each basin. We only take data at 6-h interval in IBTrACS dataset for WP, to be consistent with the 6-h interval in Extended Best Track dataset for NA and EP.

The quantity r_{17} used in this study is defined as the azimuthal-mean of the nonmissing r_{17} values when at least three of the four quadrants contain nonmissing values in best-track data. The SST associated with a given TC at each time step (denoted by TCSST) is defined as the areal weighted mean SST within a distance of r_{17} from the storm center.

The variation of the temporal-mean TCSST is large (about 4 K; e.g., Fig. 1) compared to the warming of tropical mean SST during the historical period (only ~0.5 K from ~26 °C from year 1981 to 2022). Hence, variations in observed TCSST are dominated by variations in SST relative to the tropical mean ("relative SST"). Variations in relative SST is commonly associated with weak temperature gradient (WTG) dynamics (30, 31). Thus, we define TCRSST to be TCSST minus the tropical (30°S to 30°N) mean SST of the same day for further examination of its relationship to expansion rate.

We focus on a well-behaved subset of TCs with reasonably long lifespans (here taken to be at least 5 d,* except in NA-GoM, where no threshold for lifespans is set) above tropical storm strength (maximum wind speed over 17.5 m/s) over the tropical (0 to 30°N) open ocean (TC center away from land by a distance of at least r_{17}, except for $\frac{1}{2}r_{17}$ in NA-GoM) in order to isolate cases that have a reasonable amount of time to undergo intrinsic expansion with minimal external interaction (e.g. land, extratropical transition) (16). We extract such TCs and further discard those (except those in NA-GoM) whose records of r_{17} is discontinuous when TC intensity is greater than 32 m/s and its center is equatorward of 30°N. The rest of the extracted TCs are considered of good quality and we retain only records when they are in the tropical open ocean. Then, for each of the extracted TCs, we compute the 48-h (and 24-h) expansion rate dr_{17}/dt when its maximum wind speed exceeds 32 m/s (corresponding to Category 1 hurricane). The relative SST value that corresponds to the 48-h expansion rate (denoted by rSST) is defined as the temporal average of TCRSST over the 48-h period. From these data, we calculate the maximum 48-h expansion rate of each TC. The 48-h period is taken to account for the typically slow time scale of size expansion compared to intensification (14–16, 64). Finally, we examine the dependence of maximum expansion rate as well as all valid records of expansion rates on rSSTs.†

Reanalysis Data. As a second observational test to corroborate the best-track analysis, we use the TC track and size data for NA, EP, and WP, from the 6-hourly dataset of ref. 61 where the radius of 8 m/s near surface wind (r_8) is obtained from ERA5 reanalysis (42). Reanalysis has been shown to perform well in reproducing the TC outer wind field (including radii of 6 to 8 m/s winds) as compared to satellite observations (51, 65, 66). While r_8 is a larger wind radius than r_{17}, both covary strongly together owing to the physics of the quiescent outer circulation (8, 67). TC intensity and track data are also taken from the dataset of ref. 61, which uses the National Hurricane Center source in IBTrACS for the North Atlantic and Eastern North Pacific basins and uses the Japanese Meteorological Agency source in IBTrACS for the Western North Pacific. The time period when both SST and TC data are available is 1981–2018 in NA and EP, and 1981–2019 in WP. We filter and analyze the data in an identical manner as with Best Track above, with the exception of using r_8 in lieu of r_{17}. We still use the Extended Best Track r_{17} values for the minimum distance from land threshold, except in cases (including from 1981 to 1988) when it does not exist in which case we use r_8.

Dataset of Uniform-SST-Forced Aquaplanet Simulations. For the uniform-SST aquaplanet simulations, we use the public dataset of ref. 34. They performed 11 aquaplanet simulations with globally uniform SST from 295 K to 305 K in 1 K increments. The general circulation model (GCM) they used is Community Atmosphere Model, version 5, with a horizontal grid spacing of approximately 28 km. Each experiment was run for 2 y. They tracked TCs in the experiments using the open-source TempestExtremes software package (68), which provides tracks, intensity, size, and radial wind profile of each tracked TC; these TempestExtremes-processed TC data are publicly available at ref. 69.

We apply a quality control to the TC data before analyzing the dependence of expansion rate on SST. First, we define outer size r_8 as the smallest radius (instead of the largest radius in TempestExtremes) at which the near surface wind is equal to ("greater than" in the TempestExtremes-processed TC data) 8 m/s beyond the radius of maximum wind.‡ We calculate the maximum 48-h expansion rate dr_8/dt in the same manner as the observational data with the following exceptions. First, for intensity threshold, we use a single azimuthal-mean 17 m/s intensity threshold to ensure a well-defined r_8 given that GCMs underresolve peak local wind speeds used for defining observed intensities. For each TC only the continuous segment of track that includes the timestep of lifetime maximum azimuthal-mean intensity is retained. Second, we expand our TC region to be equatorward of 40° latitude and in either hemisphere because these simulations have no large-scale temperature gradients and hence no extratropical-transition, and the simulations are hemispherically symmetric. After the above filters are applied, we retain only those cases with at least 5 d of valid data to ensure that we have a reasonably long period of time for expansion to occur. Finally, we exclude r_8 time series after peak r_8 is achieved given that TCs in these simulations can shrink at very high latitudes where they are allowed to persist unlike in nature (70).

As the records of each TC in the expansion period can be long (tens of days), composites of time series of r_8 are also calculated for each SST. A response of expansion rate to SST in this dataset should be understood in terms of global-mean warming, which is commonly associated with RCE dynamics (31); that is, environmental free-tropospheric temperature profile is essentially determined by SST (31).

*We also tested other duration thresholds: 4, and 6 d for both best-track and reanalysis data. Results do not qualitatively depend on the specific value.

†If the maximum 48-h expansion rate of a TC corresponds to several 48-h periods (which may largely overlap as seen in *SI Appendix*, Fig. S5), then we take the averaged rSST of each 48-h period as the corresponding rSST to the maximum 48-h expansion rate. The same method is applied to 24-h expansion time window.

‡This is needed as in the dataset some TCs can have multiple peaks in radial wind profile, which would cause jumps of r_8 and spurious expansion.

Historical Precipitation Dataset. For testing physical hypothesis, the historical precipitation dataset used is the Multi-Source Weighted-Ensemble Precipitation (MSWEP) precipitation dataset (40). MSWEP data are a global precipitation product with a 3-hourly 0.1° resolution available from 1979 to 2020, which incorporates gauge, satellite, radar, and reanalysis data.

Dataset for Secondary Eyewall Formation. The secondary eyewall (SE) formation dataset is from ref. 49. The dataset contains SE labels of 72 randomly selected TCs in the North Atlantic, eastern and western North Pacific, and Southern Hemisphere between 2016 and 2019. The labels also contains confidence level: "no SE, low confidence SEs (i.e., 1, 2, and 3), and high confidence SEs (i.e., 4 and 5)" (49). In order to infer whether SE occurrence and ERC is important for expansion, we use the 72 SE-labeled TCs as raw data and perform the same analysis as in Fig. 1 in the main text and separate expansion periods by whether a high-confidence SE occurs during the period.

Statistical Significance. We use *t* test to determine whether to reject the null hypothesis that the slope of a linear regression equals zero. The null hypothesis is rejected when *P*-value is less than 0.05, which means the slope is statistically significantly not zero.

Data, Materials, and Software Availability. The "Extended Best Track" data used in the study is downloaded from: https://rammb2.cira.colostate.edu/research/tropical-cyclones/tc_extended_best_track_dataset/. The IBTrACS (v04r00) data used in the study is downloaded from: https://www.ncei.noaa.gov/products/international-best-track-archive. The OISST data used in the study are downloaded from: https://rda.ucar.edu/datasets/ds277.7/dataaccess/. The reanalysis data of ref. 61 used in the study is downloaded from: http://weather.ou.edu/~schenkel/era5_size/. The aquaplanet simulation data of ref. 34 used in the study is publicly available (69) and downloaded from: https://zenodo.org/records/5764970#.ZDmVgBXMI-Q. The MSWEP data (40) used in *SI Appendix* is obtained from: https://www.gloh2o.org/mswep/. ERA5 pressure-level data (42) used in *SI Appendix* is downloaded from: https://cds.climate.copernicus.eu/datasets/reanalysis-era5-pressure-levels?tab=overview. The TC secondary eyewall dataset of ref. 49 used in *SI Appendix* is downloaded from: https://datadryad.org/stash/dataset/doi:10.5061/dryad.79cnp5j26. Scripts for generating the figures in this work are uploaded in Zenodo with a DOI: https://doi.org/10.5281/zenodo.15809707. Previously published data were used for this work (34, 40, 42, 49, 59–62).

ACKNOWLEDGMENTS. D.W. and D.R.C. were supported by NSF AGS grants 1945113 and 2431970. We acknowledge the Rosen Center for Advanced Computing at Purdue University and the Cheyenne and Derecho supercomputers (DOI: 10.5065/D6RX99HX) provided by National Center for Atmospheric Research Computational and Information Systems Laboratory for providing the data storage and computing resources to support this work. We thank the European Center for Medium-Range Weather Forecasts for access to the ECMWF (European Centre for Medium-Range Weather Forecasts) reanalysis v5 data. We thank Yuqing Wang and an anonymous reviewer for their careful reading and constructive comments that improved this work. D.W. thanks Alyssa M. Stansfield for reviewing and discussing an early version of this work.

1. M. D. Powell, T. A. Reinhold, Tropical cyclone destructive potential by integrated kinetic energy. *Bull. Am. Meteorol. Soc.* **88**, 513–526 (2007).
2. J. L. Irish, D. T. Resio, A hydrodynamics-based surge scale for hurricanes. *Ocean Eng.* **37**, 69–81 (2010).
3. Y. Lin, M. Zhao, M. Zhang, Tropical cyclone rainfall area controlled by relative sea surface temperature. *Nat. Commun.* **6**, 6591 (2015).
4. D. R. Chavas, N. Lin, W. Dong, Y. Lin, Observed tropical cyclone size revisited. *J. Clim.* **29**, 2923–2939 (2016).
5. R. E. Tuleya, M. DeMaria, R. J. Kuligowski, Evaluation of GFDL and simple statistical model rainfall forecasts for U.S. landfalling tropical storms. *Weather Forecast.* **22**, 56–70 (2007).
6. M. Paredes, B. A. Schenkel, R. Edwards, M. Coniglio, Tropical cyclone outer size impacts the number and location of tornadoes. *Geophys. Res. Lett.* **48**, e2021GL095922 (2021).
7. D. R. Chavas, N. Lin, K. Emanuel, A model for the complete radial structure of the tropical cyclone wind field. Part I: Comparison with observed structure*. *J. Atmos. Sci.* **72**, 3647–3662 (2015).
8. D. R. Chavas, N. Lin, A model for the complete radial structure of the tropical cyclone wind field. Part II. Wind field variability. *J. Atmos. Sci.* **73**, 3093–3113 (2016).
9. D. R. Chavas, J. A. Knaff, A simple model for predicting the tropical cyclone radius of maximum wind from outer size. *Weather Forecast.* **37**, 563–579 (2022).
10. C. Weatherford, W. Gray, Typhoon structure as revealed by aircraft reconnaissance. Part I. Data analysis and climatology. *Mon. Weather Rev.* **116**, 1032–1043 (1988).
11. D. R. Chavas, J. A. Knaff, P. Klotzbach, A simple model for predicting tropical cyclone minimum central pressure from intensity and size. *Weather Forecast.* **40**, 333–346 (2025).
12. P. J. Klotzbach *et al*., Characterizing continental us hurricane risk: Which intensity metric is best? *J. Geophys. Res. Atmos.* **127**, e2022JD037030 (2022).
13. B. A. Schenkel *et al*., Lifetime evolution of outer tropical cyclone size and structure as diagnosed from reanalysis and climate model data. *J. Clim.* **31**, 7985–8004 (2018).
14. K. A. Hill, G. M. Lackmann, Influence of environmental humidity on tropical cyclone size. *Mon. Weather Rev.* **137**, 3294–3315 (2009).
15. J. Martinez, C. C. Nam, M. M. Bell, On the contributions of incipient vortex circulation and environmental moisture to tropical cyclone expansion. *J. Geophys. Res. Atmos.* **125**, e2020JD033324 (2020).
16. D. Wang, D. R. Chavas, An analytical model for tropical cyclone outer-size expansion on the f plane. *J. Atmos. Sci.* **81**, 1097–1125 (2024).
17. A. J. Garner, Observed increases in north Atlantic tropical cyclone peak intensification rates. *Sci. Rep.* **13**, 16299 (2023).
18. K. Bhatia *et al*., A potential explanation for the global increase in tropical cyclone rapid intensification. *Nat. Commun.* **13**, 6626 (2022).
19. H. A. Ramsay, M. S. Singh, D. R. Chavas, Response of tropical cyclone formation and intensification rates to climate warming in idealized simulations. *J. Adv. Model. Earth Syst.* **12**, e2020MS002086 (2020).
20. K. Emanuel, Will global warming make hurricane forecasting more difficult? *Bull. Am. Meteorol. Soc.* **98**, 495–501 (2017).
21. K. Bhatia, G. Vecchi, H. Murakami, S. Underwood, J. Kossin, Projected response of tropical cyclone intensity and intensification in a global climate model. *J. Clim.* **31**, 8281–8303 (2018).
22. K. Emanuel, Self-stratification of tropical cyclone outflow. Part II. Implications for storm intensification. *J. Atmos. Sci.* **69**, 988–996 (2012).
23. Y. Wang, Y. Li, J. Xu, A new time-dependent theory of tropical cyclone intensification. *J. Atmos. Sci.* **78**, 3855–3865 (2021).
24. Y. Wang, Y. Li, J. Xu, Z. M. Tan, Y. Lin, The intensity dependence of tropical cyclone intensification rate in a simplified energetically based dynamical system model. *J. Atmos. Sci.* **78**, 2033–2045 (2021).
25. Y. Wang, Z. M. Tan, Y. Li, Some refinements to the most recent simple time-dependent theory of tropical cyclone intensification and sensitivity. *J. Atmos. Sci.* **80**, 321–335 (2023).
26. K. Emanuel, R. Rotunno, Self-stratification of tropical cyclone outflow. Part I. Implications for storm structure. *J. Atmos. Sci.* **68**, 2236–2249 (2011).
27. Y. Sun *et al*., Impact of ocean warming on tropical cyclone size and its destructiveness. *Sci. Rep.* **7**, 8154 (2017).
28. Y. Li, Y. Wang, Y. Lin, R. Fei, Dependence of superintensity of tropical cyclones on SST in axisymmetric numerical simulations. *Mon. Weather Rev.* **148**, 4767–4781 (2020).
29. N. Bruneau, S. Wang, R. Toumi, Long memory impact of ocean mesoscale temperature anomalies on tropical cyclone size. *Geophys. Res. Lett.* **47**, e2019GL086165 (2020).
30. A. H. Sobel, J. Nilsson, L. M. Polvani, The weak temperature gradient approximation and balanced tropical moisture waves. *J. Atmos. Sci.* **58**, 3650–3665 (2001).
31. H. A. Ramsay, A. H. Sobel, Effects of relative and absolute sea surface temperature on tropical cyclone potential intensity using a single-column model. *J. Clim.* **24**, 183–193 (2011).
32. K. Emanuel, Inferences from simple models of slow, convectively coupled processes. *J. Atmos. Sci.* **76**, 195–208 (2019).
33. O. Peters, J. D. Neelin, Critical phenomena in atmospheric precipitation. *Nat. Phys.* **2**, 393–396 (2006).
34. A. M. Stansfield, K. A. Reed, Tropical cyclone precipitation response to surface warming in aquaplanet simulations with uniform thermal forcing. *J. Geophys. Res. Atmos.* **126**, e2021JD035197 (2021).
35. Y. Li, Y. Tang, S. Wang, Rapid growth of outer size of tropical cyclones: A new perspective on their destructive potential. *Geophys. Res. Lett.* **49**, e2022GL099230 (2022).
36. Y. Li, Y. Tang, S. Wang, X. Li, Rapid growth of tropical cyclone outer size over the western north pacific. *Remote Sens.* **15**, 486 (2023).
37. Y. Wang, How do outer spiral rainbands affect tropical cyclone structure and intensity? *J. Atmos. Sci.* **66**, 1250–1273 (2009).
38. H. Fudeyasu, Y. Wang, Balanced contribution to the intensification of a tropical cyclone simulated in TCM4: Outer-core spinup process. *J. Atmos. Sci.* **68**, 430–449 (2011).
39. J. Xu, Y. Wang, Sensitivity of the simulated tropical cyclone inner-core size to the initial vortex size. *Mon. Weather Rev.* **138**, 4135–4157 (2010).
40. H. E. Beck *et al*., Mswep v2 global 3-hourly 0.1 ° precipitation: Methodology and quantitative assessment. *Bull. Am. Meteorol. Soc.* **100**, 473–500 (2019).
41. L. Qin *et al*., Global expansion of tropical cyclone precipitation footprint. *Nat. Commun.* **15**, 4824 (2024).
42. H. Hersbach *et al*., The ERA5 global reanalysis. *Q. J. R. Meteorol. Soc.* **146**, 1999–2049 (2020).
43. D. R. Chavas, K. Emanuel, Equilibrium tropical cyclone size in an idealized state of axisymmetric radiative-convective equilibrium*. *J. Atmos. Sci.* **71**, 1663–1680 (2014).
44. K. J. E. Walsh *et al*., Real world and tropical cyclone world. Part II: Sensitivity of tropical cyclone formation to uniform and meridionally varying sea surface temperatures under aquaplanet conditions. *J. Clim.* **33**, 1473–1486 (2020).
45. J. P. Kossin, M. Sitkowski, An objective model for identifying secondary eyewall formation in hurricanes. *Mon. Weather Rev.* **137**, 876–892 (2009).
46. M. Sitkowski, J. P. Kossin, C. M. Rozoff, Intensity and structure changes during hurricane eyewall replacement cycles. *Mon. Weather Rev.* **139**, 3829–3847 (2011).
47. Y. H. Huang, M. T. Montgomery, C. C. Wu, Concentric eyewall formation in typhoon sinlaku (2008). Part II: Axisymmetric dynamical processes. *J. Atmos. Sci.* **69**, 662–674 (2012).
48. X. Yang, Y. Wang, H. Wang, J. Xu, R. Zhan, Effect of the initial vortex structure on intensity change during eyewall replacement cycle of tropical cyclones: A numerical study. *J. Trop. Meteorol.* **30**, 106–117 (2024).

49. A. A. Cheung, C. J. Slocum, J. A. Knaff, M. N. Razin, Documenting the progressions of secondary eyewall formations. *Weather Forecast.* **39**, 19–40 (2024).
50. H. C. Kuo, C. P. Chang, Y. T. Yang, H. J. Jiang, Western north pacific typhoons with concentric eyewalls. *Mon. Weather Rev.* **137**, 3758–3770 (2009).
51. B. A. Schenkel *et al*., North Atlantic tropical cyclone outer size and structure remain unchanged by the late twenty-first century. *J. Clim.* **36**, 359–382 (2023).
52. K. Y. Lu, D. R. Chavas, Tropical cyclone size is strongly limited by the Rhines scale: Experiments with a barotropic model. *J. Atmos. Sci.* **79**, 2109–2124 (2022).
53. A. H. Sobel *et al*., Near-term tropical cyclone risk and coupled earth system model biases. *Proc. Natl. Acad. Sci. U.S.A.* **120**, e2209631120 (2023).
54. J. Molinari, D. Vollaro, External influences on hurricane intensity. Part I: Outflow layer eddy angular momentum fluxes. *J. Atmos. Sci.* **46**, 1093–1105 (1989).
55. S. Nong, K. Emanuel, A numerical study of the genesis of concentric eyewalls in hurricanes. *Q. J. R. Meteorol. Soc.* **129**, 3323–3338 (2003).
56. K. Liu, J. C. Chan, Synoptic flow patterns associated with small and large tropical cyclones over the western North Pacific. *Mon. Weather Rev.* **130**, 2134–2142 (2002).
57. K. T. Chan, J. C. Chan, Angular momentum transports and synoptic flow patterns associated with tropical cyclone size change. *Mon. Weather Rev.* **141**, 3985–4007 (2013).
58. K. S. Maclay, M. DeMaria, T. H. Vonder Haar, Tropical cyclone inner-core kinetic energy evolution. *Mon. Weather Rev.* **136**, 4882–4898 (2008).
59. B. Huang *et al*., Improvements of the daily optimum interpolation sea surface temperature (DOISST) version 2.1. *J. Clim.* **34**, 2923–2939(2021).
60. K. R. Knapp, M. C. Kruk, D. H. Levinson, H. J. Diamond, C. J. Neumann, The international best track archive for climate stewardship (IBTRACS) unifying tropical cyclone data. *Bull. Am. Meteorol. Soc.* **91**, 363–376 (2010).
61. A. Gori, N. Lin, B. Schenkel, D. Chavas, North atlantic tropical cyclone size and storm surge reconstructions from 1950-present. *J. Geophys. Res. Atmos.* **128**, e2022JD037312 (2023).
62. J. L. Demuth, M. DeMaria, J. A. Knaff, Improvement of advanced microwave sounding unit tropical cyclone intensity and size estimation algorithms. *J. Appl. Meteorol. Climatol.* **45**, 1573–1581 (2006).
63. J. A. Knaff *et al*., Estimating tropical cyclone surface winds: Current status, emerging technologies, historical evolution, and a look to the future. *Trop. Cyclone Res. Rev.* **10**, 125–150 (2021).
64. D. Wang, Y. Lin, D. R. Chavas, Tropical cyclone potential size. *J. Atmos. Sci.* **79**, 3001–3025 (2022).
65. B. A. Schenkel, N. Lin, D. Chavas, M. Oppenheimer, A. Brammer, Evaluating outer tropical cyclone size in reanalysis datasets using QuikSCAT data. *J. Clim.* **30**, 8745–8762 (2017).
66. G. F. Bian, G. Z. Nie, X. Qiu, How well is outer tropical cyclone size represented in the ERA5 reanalysis dataset? *Atmos. Res.* **249**, 105339 (2021).
67. K. Emanuel, "Tropical cyclone energetics and structure" in *Atmospheric Turbulence and Mesoscale Meteorology*, E. Fedorovich, R. Rotunno, B. Stevens, Eds. (Cambridge University Press, 2004), pp. 165–191.
68. P. A. Ullrich, C. M. Zarzycki, Tempestextremes: A framework for scale-insensitive pointwise feature tracking on unstructured grids. *Geosci. Model Dev.* **10**, 1069–1090 (2017).
69. R. K. Stansfield, A Cam global RCE simulations TC track, radial profiles, and filtered precipitation files. Zenodo. (2021), 10.5061/dryad.x3ffbg7jv. Accessed 30 April 2023.
70. D. R. Chavas, K. A. Reed, Dynamical aquaplanet experiments with uniform thermal forcing: System dynamics and implications for tropical cyclone genesis and size. *J. Atmos. Sci.* **76**, 0001.1 (2019).